Published in final edited form as:
Macromolecules. 2012 June 12; 45(11): 4572–4580. doi:10.1021/ma2024914.

Nanopatterned Protein Films Directed by Ionic Complexation with Water-Soluble Diblock Copolymers

Bokyung Kim, **Christopher N. Lam**, and **Bradley D. Olsen***
Department of Chemical Engineering, Massachusetts Institute Technology, 77 Massachusetts Avenue, Cambridge, Massachusetts 02139, United

Abstract

The use of ionic interactions to direct both protein templating and block copolymer self-assembly into nanopatterned films with only aqueous processing conditions is demonstrated using block copolymers containing both thermally responsive and pH responsive blocks. Controlled reversible addition-fragmentation chain-transfer (RAFT) polymerization is employed to synthesize poly(*N*-isopropylacrylamide-*b*-2-(dimethylamino)ethyl acrylate) (PNIPAM-*b*-PDMAEA) diblock copolymers. The pH-dependent ionic complexation between the fluorescent protein, mCherry, and the ionic PDMAEA block is established using dynamic light scattering (DLS) and UV-Vis spectroscopy. DLS shows that the size of the resulting coacervate micelles depends strongly on pH, while UV-Vis spectroscopy shows a correlation between the protein's absorption maximum and the ionic microenvironment. Zeta potential measurements clearly indicate the ionic nature of the complex-forming interactions. Spin casting was used to prepare nanostructured films from the protein-block copolymer coacervates. After film formation, the lower critical solution temperature (LCST) of the PNIPAM blocks allows the nanomaterial to be effectively immobilized in aqueous environments at physiological temperatures, enabling potential use as a controlled protein release material or polymer matrix for protein immobilization. At pH 9.2 and 7.8, the release rates are at least 10 times faster than that at pH 6.4 due to weaker interaction between protein and PNIPAM-*b*-PDMAEA (PND) diblock copolymer. Due to the ionic environment in which protein is confined, the majority of the protein (80%) remains active, independent of pH, even after having been dehydrated in vacuum and confined in the films.

Keywords

Stimuli-sensitive polymer; Block copolymer; Self-assembly; Protein delivery

INTRODUCTION

The rapid progress of nanotechnology in protein-polymer hybrids calls for better defined and more finely tuned nanostructures, allowing high density three-dimensional structures to

*Corresponding Author: Bradley D. Olsen, TEL) 1-617-715-4548, bdolsen@mit.edu.

SUPPORTING INFORMATION
Gel permeation chromatography (GPC) and nuclear magnetic resonance (NMR) data of PND block copolymer, and calibration curves for determining released and remaining mCherry concentrations. This material is available free of charge via the Internet at http://pubs.acs.org.

be produced that have improved protein activity and stability.[1–3] For many biomedical and biotechnological applications including biosensors,[4–7] fuel cells, [8–10] biocatalysts,[11–13] photovoltaics,[14–15] and patterns for cell growth,[16–17] control over the nanostructure of the protein-containing material is critical to improving the performance of the final device. Historically, conventional techniques for manufacturing materials with desired functionalities on the nanometer scale have involved different top-down methods such as electron-beam writing and dip-pen lithography.[18–19] Some groups have also taken a hybrid top-down and bottom-up approach to obtain control over larger areas. For example, patterning of metallic nanoparticles on a silicon substrate was achieved by combining the self-assembly of nanoparticlebinding protein molecules with a lithographically manufactured hydrophobic surface.[20] Additionally, the joint use of nanoimprint lithography and molecular assembly patterning by lift-off results in streptavidin patterns on the order of 100 nm.[21] Constantly improving synthetic techniques have also made the synthesis of protein-polymer diblocks feasible, opening the possibilities of a bottom-up approach based on direct self-assembly of the protein. Through intelligent design of the bioconjugate, these protein-polymer block copolymers may be self-assembled in a controlled fashion in the solid state[22] and in solution.[23–24]

Block copolymer templating provides a bottom-up method for the three-dimensional patterning of proteins within a controlled nanoscale environment that does not rely on often challenging bioconjugation techniques. Furthermore, control over the nanoscale protein environment in the template has the potential to improve protein activity and stability within a solid material. Block copolymers microphase separate into well-defined microdomains that are typically tens of nanometers in size,[25–28] large enough to serve as a scaffold to confine proteins, which are typically less than 5 nm.[29] One fundamental advantage of the polymer template approach to protein-polymer hybrid materials is the combination of the protein's specific biological function with the bulk properties and processability of synthetic block copolymers. Previously demonstrated strategies for block copolymer templating have relied primarily on nonspecific hydrophobic interactions to drive self-assembly. Nonspecific hydrophobic interactions enable differential adsorption of proteins onto nanopatterned domains on two-dimensional surfaces of polymer thin films,[30–32] and protein-poly(ethylene glycol) (PEG) conjugates have been employed to direct proteins into specific nanodomains of a polystyrene-*b*-poly(ethylene oxide) block copolymer by casting from organic solvents.[2] In addition, hydrophobic interactions may be used to template membrane proteins with small molecule or block copolymer surfactants.[33–34]

Employing water-soluble block copolymers as templates would potentially extend the utility of templated self-assembly by allowing hybrid block copolymer-protein films to be prepared from soluble proteins in an aqueous environment where a wide variety of proteins maintain their native folding and enzymatic functionality. This presents two challenges: first, since both blocks of the block copolymer and the protein are soluble in water, new interactions must be found to drive self-assembly. Second, the templated structures must be engineered for use in an aqueous environment without dissolving. Ionic interactions provide a water-compatible method for directing protein-block copolymer self-assembly. The self-assembly of coacervate micelles has been demonstrated due to attractive interactions between a

protein and the ionic block of a block copolymer containing both ionic and nonionic blocks.[35–37] The charge on the ionic block and the protein can be controlled by tuning the solution pH, which affects the strength of the protein-block copolymer complexation.[38–39] In order to develop materials that are processable in water but maintain structural integrity during application in water, a thermoresponsive nonionic polymer block can be used. Above the lower critical solution temperature (LCST) of the thermoresponsive polymer, the polymer block will collapse and precipitate out of the aqueous solution.[40–41] In a thin film, the solubility transition of the thermoresponsive block may result in the formation of an insoluble film at elevated temperatures.

This work uses these ionic interactions to demonstrate a new method for templating protein selfassembly in solid thin films using all aqueous processing. Ionic interactions between proteins and block copolymers are used to drive self-assembly, while a thermoresponsive polymer block enables films to be made hydrophobic for stable use in aqueous environments after fabrication. Block copolymers containing poly(2-(dimethylamino)ethyl acrylate) (PDMAEA) and poly(*N*-isopropylacrylamide) (PNIPAM) are synthesized by reversible addition-fragmentation chain transfer (RAFT) polymerization and used to prepare nanostructured templates. mCherry is selected as a model protein for complexation because of its high-yield expression in *Escherichia coli* (*E. coli*), its well-established purification, and its fluorescent nature that provides a simple and robust spectrophotometric assay method for functionality and spatial distribution within solid materials. Ionic complexes between mCherry and PNIPAM-*b*-PDMAEA (PND) diblock copolymers are formed in an aqueous system of varying pH prior to casting of self-assembled protein-block copolymer hybrid films, as presented in Figure 1. Proteinblock copolymer hybrid films are prepared through water-based self-assembly and coating onto planar substrates using volatile acids and bases to vary the solution pH. Above the LCST of PNIPAM the films become water insoluble, and the activity of mCherry in films and the pH-dependent release of protein are measured, illustrating the utility of these templates both as stable biofunctional materials and as controlled release coatings.

EXPERIMENTAL SECTION

Polymerization

RAFT polymerization[42] was used to synthesize diblock copolymers from *N*-isopropylacrylamide (NIPAM) (98%, TCI) and 2-(dimethylamino)ethyl acrylate (DMAEA) (99%, Aldrich) with a narrow molecular weight distribution. NIPAM was sublimed at 55 °C under vacuum and DMAEA was passed through a basic alumina column prior to polymerization to remove inhibitors. 2-Dodecylsulfanythiocarbonysulfanyl-2-methyl propionic acid (DMP) was prepared as the RAFT chain transfer agent, following the work of You and Oupicky.[43] DMP and azobisisobutyronitrile (AIBN, recrystallized twice from methanol) were added to a 2.0 M solution of NIPAM in 10 ml of 1,4-dioxane in the ratio 500 : 1 : 0.2 (monomer : CTA : initiator). The solution was degassed by three freeze– pump–thaw cycles. The polymerization was carried out in a sealed flask at 60 °C and terminated after 3 hours by removal of heat and exposure to oxygen. The polymer was then precipitated in cold diethyl ether and dried under vacuum. The PNIPAM homopolymer (M_n = 42 kg/mol,

PDI = 1.1) obtained was used as a macromolecular chain transfer agent for RAFT polymerization of DMAEA. DMAEA and AIBN were added to PNIPAM solution in 15 ml of 1,4-dioxane in the ratio 1000 : 1 : 0.3 (monomer : CTA : initiator). The polymerization was carried out in a sealed flask at 60 °C and terminated after 24 hr. by removal of heat and exposure to oxygen. The polymer was then precipitated in *N*-hexane and dried under vacuum. The polymerization provided a well-defined PNIPAM-*b*-PDMAEA (PND) diblock copolymer of molecular weight M_n = 57 kg/mol with PDI of 1.12. A PNIPAM-rich molecular composition was chosen in order to promote the formation of soluble coacervate micelles. The molecular weights and polydispersities were determined by gel permeation chromatography using a Waters Breeze 1525 HPLC system with a series 2414 refractive index detector, calibrated with poly(methyl methacrylate) standards, and *N*,*N*-dimethylformamide with 0.01 M LiBr was used as the mobile phase.

Protein Expression

A gene encoding for a 6xHis-tagged variant of mCherry was cloned into the vector pQE9 (Qiagen) and transformed into *E. coli* strain SG13009 containing the pREP4 repressor plasmid. Cultures were grown in Terrific Broth at 37 °C, and protein expression was induced with 1 mM isopropyl β-d-1-thiogalactopyranoside (IPTG) at OD_{600} = 1. The cells were cultured for 4.5 h after induction and were then harvested. The cells were resuspended in lysis buffer (50 mM NaH_2PO_4, 300 mM sodium chloride, 10 mM imidazole, pH 8.0), incubated with 1 mg/mL lysozyme at 4 °C for 30 min, and sonicated. The lysate was clarified, and the protein was purified using nickel-nitrilotriacetic acid (Ni–NTA) metal affinity chromatography. Elution fractions containing purified protein were dialyzed into milli-Q water. The yield of purified protein, determined spectrophotometrically at 586 nm based on the known extinction coefficient of mCherry,[44] was 121 mg/L culture.

Characterization

Ionic complexes between mCherry and PND diblock were characterized in aqueous solution by zeta potential, dynamic light scattering (DLS) and UV-Vis spectroscopy. Hydrochloric acid (HCl) and ammonium hydroxide (NH_4OH) were used to vary the pH of the solutions. Zeta potential (Brookhaven Zeta PALS) was studied to determine the net surface charge calculated by electrophoretic mobility of samples as a function of pH in salt-free aqueous solution. Dynamic light scattering (DLS) (DynaPro Titan) was used to determine the sizes and polydispersity of the coacervate micelles at a scattering angle of 90° and at a temperature of 25 °C. The samples were illuminated by an 830 nm semiconductor laser, above the absorption band of mCherry to minimize inelastic scattering. UV–Vis spectra were collected on a Cary 50 UV–Vis spectrophotometer with Peltier thermal controller using a quartz cuvette. All samples were characterized at a polymer concentration of 1 mg/mL.

For the surface imaging of hybrid films, 2 wt.% solutions of mCherry and PND were spin cast onto Si wafers pretreated with oxygen plasma. An Asylum MFP-3D SFM was used to image samples in tapping mode with a tip with resonant frequency ~300 kHz (Tap300-G, Budjetsensors). The thickness of the film was measured by spectroscopic ellipsometry

(M-2000, Woolham) at a fixed angle of 70° with varying wavelength of 300–900 nm. The thickness of the films was determined by fitting the resulting data using the Cauchy model.

The LCST or the cloud point was determined by turbidity measurements on the Cary 50 UV–Vis spectrophotometer with Peltier thermal controller using a quartz cuvette. LCST, where the PNIPAM blocks become insoluble, was quantified as the 50% transmittance point in the heating curve. Transmission is measured at 450 nm, outside the absorption band of mCherry, at a sweep rate of 0.2 °C/min. Samples were measured at a polymer concentration of 1 wt.% and a molar ratio of polymer to protein $r_m = 14.2$. Optical activity assays of mCherry released from the hybrid films were performed to quantify the functionality of released protein. Films with an area of 4 cm^2 and an average thickness of 200 nm were spin cast from pH 6.4 aqueous solutions and estimated to contain 1.3 nmol of mCherry based on the initial mCherry concentration in solution and the measured film thickness. To preserve the film structure, samples were immersed into 10 mM sodium phosphate buffer kept at 40 °C, above the LCST of PNIPAM in the PND and mCherry system. The fluorescence intensity of the buffer was measured as a function of time using a plate reader (Varioskan Flash, Thermo Scientific) at 610 nm to calculate the concentration of released mCherry based on a separate calibration curve for each pH. After 4 hours, samples were cooled down to 25 °C, where the remaining film was totally dissolved into fresh buffer. Once again, the fluorescence intensity of the buffer was measured to calculate the concentration of mCherry remaining in the film after the release experiment. The amount of inactive mCherry was calculated by subtracting the released and remaining active mCherry concentrations from the initial concentration of mCherry added to the film.

RESULTS AND DISCUSSION

Characterization of Ionic Complexation in Solution

The types and extent of mCherry-PND interactions can be categorized into three separate regimes defined by the isoelectric point of the protein (pI = 6.0)[45] and the acid dissociation constant of the amino group in the PDMAEA block ($pK_{a,monomer} = 8.6$).[46] By titration with dilute HCl, the acid dissociation constant of PDMAEA was determined to be $pK_{a,PDMAEA} = 8.5$, similar to the monomer's literature value. Figure 2a shows that the positive net surface charge of mCherry decreases with increase in the pH of the solution and crosses from positive to negative at pH 5.8, close to the pI value of mCherry. The positive net charge of protonated PND also decreases with increase in pH, dropping to nearly zero above $pK_{a,PDMAEA}$ as the amine groups become deprotonated. Therefore, under conditions of $pI < pH < pK_{a,PDMAEA}$ at a molar ratio of polymer to protein $r_m = 14.2$, protonated amine pendant groups lead to relatively strong complexation with the proteins due to opposite net charges. The resulting complexes have a net positive charge, although significantly lower than that of the block copolymer. This value of the molar ratio was chosen because it is near optimum for immobilization and nanotemplating in thin films.

At pH conditions greater than the pK_a value of the polymer, the PDMAEA amino groups are mostly in their deprotonated base form, and mCherry has a net negative surface charge. Therefore, relatively weak Coulombic interactions are expected. In the high pH regime, DLS data, shown in Figure 2b, indicate that the interaction between mCherry and PND results in

particle sizes of 21 to 23 nm, consistent with the anticipated weak interactions. This observed complexation between PND and mCherry under highly basic conditions may result from a combination of relatively weak hydrogen bonding between the uncharged PDMAEA amino groups and protonated amino acid residues and relatively weak Coulombic interactions between the small number of protonated DMAEA residues and the negative protein surface charges. At higher pH values, one would expect that the number of protein-PND associations due to hydrogen bonding and electrostatic interactions decreases, consistent with the observed trend of decreasing particle diameter with increasing pH. The second significant pH range falls between the mCherry isoelectric point of 6.0 and the PDMAEA acid dissociation constant of approximately $pK_{a,PDMAEA} = 8.5$. Within this pH range, relatively strong electrostatic interactions exist between the protonated amino groups in the block copolymer and the net negative surface charge of the protein, leading to the formation of coacervate micelles. DLS measurements confirm a large increase in particle diameter from 23 nm at pH = 7.9 to 40 nm at pH = 6.4. The third pH regime corresponds to pH values lower than the protein isoelectric point. In this regime, both the protein and the block copolymer have a positive charge. However, DLS indicates a continued gradual increase in micelle diameter with further decrease in pH. This increase in size may be attributed to proton migration within the protein[47] which can result in an induced negative charge at the protein surface because the charges are labile. This can lead to multiple low-energy complexation states even when the global protein and block copolymer charges are repulsive.

Neither mCherry nor block copolymer solutions show strongly pH-dependent size effects. DLS measurements of mCherry in Figure 2b confirm that its size of approximately 4 nm is relatively invariant across a wide range of pH. Similarly, DLS results show that PND is not affected significantly by its pH environment, measuring approximately 13 nm. Comparing pH < 6 and pH > 8, the size of PND is observed to increase from 10 to 14 nm, a small increase which can be attributed to repulsive forces between the protonated PND blocks that cause extended chain configurations. Therefore, the significant increase in particle size in mCherry/PND blends with decreasing pH is governed by interactions between mCherry and the block copolymer.

The large effect of ionic association on complex formation below the pK_a of PDMAEA is illustrated by DLS experiments at variable ionic strength. Figure 2c shows the aggregate sizes measured by DLS in 10 and 50 mM salt concentrations. For pH > 8.0, an approximately 5% decrease was observed in aggregate size upon increasing from 0 to 10 mM sodium phosphate, with little change observed between 10 and 50 mM. This minor difference between buffered and salt-free conditions is consistent with weak, nonionic interactions. For pH < 8.0, there is a much larger 33% decrease in the coacervate diameter as the salt concentration is increased from 0 to 10 mM sodium phosphate, again with little change upon further increase to 50 mM. The much larger effect of salt at low pH confirms the role of strong electrostatic interactions governing the formation of coacervates, as the salt ions have a larger screening effect than at higher pH where weaker interactions are dominant. The absence of further size change upon increasing from 10 to 50 mM sodium phosphate is explained by the Debye lengths of 1.24 and 0.56 nm at 10 and 50 mM, respectively. These lengths are shorter than the protein radius of gyration and of the order of

the typical polymer Kuhn length,[48] suggesting that further electrostatic screening from increasing salt concentration has a minimal effect on association.

UV-Vis measurements of mCherry-PND complexes show shifts in the absorption maximum of mCherry, confirming the formation of electrostatic complexes between mCherry and the PDMAEA block. mCherry has a β-barrel structure that isolates its chromophore from the exterior, and thus the optical properties and stability depend on the amino acid residues forming the chromophore and those in its immediate vicinity.[49–50] Figure 3 shows that the absorbance maxima of mCherry are strongly pHdependent, exhibiting a blue shift from 587 to 566 nm with increasing pH from 6.4 to 11.4. It has previously been shown that under increasingly basic environments, deprotonation of G215, the glutamic acid residue near the mCherry chromophore, results in more pronounced blue shifting of the mCherry maximum absorption peak.[50] In contrast, in the presence of PND, red shifts are observed from 569 to 587 nm as pH increases, supporting the formation of a complexation between mCherry and PND. In particular, at pH 11.4 where the coacervate size is a minimum by DLS and interactions are expected to be relatively weak, there is a blue shift of 21 nm relative to the protein in the absence of PND. Although the primary absorbance peak shifts in opposite directions with increasing pH with and without the presence of PND, in both cases the molar absorptivity is observed to reversibly decrease with decreasing pH. Spectrophotometric measurements of mCherry as a function of pH also show the presence of a secondary absorbance peak at 449 nm at pH 6.4. The underlying mechanism resulting in this second absorption peak is different altogether from that causing the blue shifting of the primary absorption peak at higher pH conditions. The presence of two absorption bands has been attributed to the phenol and phenolate transition in the chromophore of GFP[51] and of a red fluorescent protein mKeima[52]. The mCherry chromophore comprises the amino acid triplet of residues Q66, Y67, and G68, and two separate ground states of mCherry corresponding to the phenol and phenolate conformation of the tyrosine residue at acidic and basic conditions lead to the observed two absorption peaks at 449 and 568 nm, respectively. Comparing the spectra of mCherry and that of mCherry-PND at a pH of 6.4 reveals that in the presence of PND, interaction between the protein and block copolymer prevents the formation of the peak at 449 nm observed for mCherry at pH = 6.4. This effect of PND in suppressing protonation of the tyrosine in the chromophore further indicates the role of PND in promoting negative charge on mCherry around its isoelectric point.

Templating Protein Self-Assembly into Block Copolymer Thin Films

Casting films from the mCherry-PND complexes results in the formation of nanostructured block copolymer templates with mCherry segregated in the PDMAEA nanodomains. Figure 4 shows scanning force microscopy (SFM) images of the hybrid films cast from 2 wt.% solutions (r_m = 14.2) at pH 6.4 and 9.2. The thicknesses of the resulting films are 41 and 43 nm, measured by spectroscopic ellipsometry. Both films are smooth, with an average mean square roughness (R_a) of 1.3 and 0.5 nm, respectively. In Figure 4 (a), the surface morphology of the film cast at pH 6.4 shows disordered spherical nanodomains in the height image with 42 nm domain spacing as measured using fast Fourier transforms (FFT) of the SFM image. From the interdomain spacing of the micelles from the FFT in Figure 4a at pH = 6.4 and r_m = 14.2, the number of mCherry molecules templated in the PDMAEA domain

was determined to be approximately 35. At pH = 6.4, aggregation of primary complexes formed from relatively strong ionic interactions between negative protein surface charges and positive charges of protonated PDMAEA result in coacervates 40 nm in diameter in solution, in close agreement with the domain spacing measured in the film.

The transition from spherical micelles to shallow pores during casting suggests that the cores in the micelles are swollen with water until after the glassy PNIPAM domains have vitrified, resulting in collapse of the micellar core to form a depression during the later stages of film drying. Although water is not a selective solvent in these block copolymers, the ionic nanodomains are expected to have a significantly higher osmotic pressure than the nonionic domains, leading to removal of water from the PNIPAM domains before the PDMAEA domains and forming a dimple structure at the air interface. As shown in Figure 4c, the surface of the hybrid film cast pH 9.2 is flat, and nanodomain features are not well-developed. This is consistent with the weaker interactions between PDMAEA and mCherry for pH > 8, indicating that templated self-assembly requires relatively strong ionic interactions. It is also hypothesized that the Flory-Huggins interaction parameter, χ, may be smaller for interactions between neutral PDMAEA and PNIPAM than the corresponding value for interactions between protonated PDMAEA and PNIPAM; therefore, good contrast between the nanodomains is not observed.

The localization of mCherry within nanodomain structures, as opposed to macrophase separation from the block copolymer, is clearly illustrated by fluorescence microscopy, as shown in Figure 5. A comparison between PNIPAM/PDMAEA blends and PND block copolymers shows a dramatic difference between the sizes of the phase-separated domains with the selective complexation of mCherry. In Figures 5a and b, both fluorescence and bright-field images of the blend film containing r_m = 14.2 mCherry loading shows a macrophase separated morphology with a characteristic length scale for phase separation typically tens of micrometers in size for blends with equal mass of PNIPAM and PDMAEA. Microphase separation of mCherry from PNIPAM has also been observed in self-assembled protein-polymer conjugates,[22] suggesting that PNIPAM and mCherry are poorly miscible. The cationic PDMAEA at pH = 6.4 has strong electrostatic interactions with mCherry, resulting in solubilization of mCherry within the PDMAEA and phase separation of mCherry-rich PDMAEA regions from PNIPAM. However, as shown in Figures 5c and d, mCherry seems to be homogeneously distributed on the PND block copolymer films since mCherry is confined in PDMAEA microdomains, tens of nanometers in size, which are invisible by optical microscopy.

Either increasing the mCherry loading or weakening the ionic interactions by increasing the casting solution pH may induce macrophase separation when the capacity of the block copolymer template is exceeded. In Figure 5e, fluorescence microscopy reveals a predominantly homogeneous distribution of mCherry for PND films cast at pH = 6.4 with r_m = 2.8, but a number of regions resembling hairline fractures are observed to exhibit intense fluorescence. At this high mCherry loading amount, the excess mCherry is unable to complex with the PDMAEA block and aggregates to form inhomogeneities. Molar ratios of polymer to mCherry ranging from r_m = 2.8 to 14.2 at pH = 6.4 were studied to determine the maximum amount of mCherry that is solubilized in the core PDMAEA block, indicating a

maximum loading between r_m = 11.1 and 14.2. As the ratio of PND to mCherry increases in the film, the fracture-like structures and bright spots decrease in number, suggesting a lower volume fraction of phase separated mCherry at increasing r_m. The 2 wt.% casting solutions exhibited no signs of turbidity, suggesting that macrophase separation occurs during the casting process due to phase segregation of uncomplexed mCherry from the block copolymer. At a higher pH = 9.2 with r_m = 14.2, mCherry macrophase separation also occurs. Under this basic pH condition, relatively weak Coulombic interactions between the mCherry and PDMAEA block are insufficient to complex all of the protein to the block copolymer, leading to aggregates that appear as diffuse, inhomogeneous structures with discrete bright spots, as shown in Figure 5f. Therefore, there is a pH-dependent capacity of the block copolymer template, governed by the strength of the ionic interactions.

Protein Activity and Film Stability

In order to allow the aqueous-processed template films to be used in aqueous environments without dissolving, the films are heated above the LCST of the PNIPAM block to make the majority nanodomain insoluble, while the ionic complexation between PDMAEA and mCherry results in insolubility of the minority nanodomains. Figure 6 shows the effect of pH on the thermosensitive solubility of PNIPAM homopolymers, PND block copolymer, and mCherry-PND complexes in 10 mM sodium phosphate buffer. The LCST or the cloud point, where the PNIPAM blocks become insoluble, was quantified as the 50% transmittance point in the heating curve. In Figure 6a, the LCST of PNIPAM homopolymers shows a weak pH dependence, as it decreases from 33.6 to 32.5 °C. Sharp transitions are observed at all pH values due to the breakage of hydrogen bonds between water and amide groups. As previously reported, the slight ionization of PNIPAM under strongly basic conditions[53] promotes an inhibited collapse behavior of the more hydrophilic PNIPAM. Figure 6b shows that the existence of non-temperature-sensitive but water-soluble PDMAEA blocks causes an increase in the LCST of PNIPAM. It is well-established that the thermoresponsive transition of block copolymers containing PNIPAM strongly depends on the hydrophobicity/hydrophilicity of the other block, with hydrophobic blocks depressing the LCST of PNIPAM and hydrophilic blocks increasing the LCST.[54] It is expected that at lower pH conditions, the protonated and more hydrophilic PDMAEA block would result in a higher LCST relative to that of the block copolymer at higher pH conditions. However, the opposite is observed, with the largest increase in LCST occurring at high pH when the PDMAEA block is predominantly in its deprotonated state. It is also interesting to note the diffuse character of the thermoresponsive transition at this basic condition, which could be a result of kinetic effects of PNIPAM aggregation above the transition point. The thermoresponsive transitions of the PND block copolymer and of the mCherry-PND coacervates display much greater pH-dependence than that of homopolymer PNIPAM, as is expected based on the pH sensitivity of the PDMAEA block. Cloud point transitions of PND at pH = 9.2 and of PND with mCherry at pH 9.2 and 7.8 become more diffuse and has two inflection points, which is uncharacteristic for a thermoresponsive polymer. For the mCherry-PND solution at pH 6.4, however, the transition is very sharp and has a low LCST of 31.0°C, as can be seen in Figure 6c. Once the pH is lowered into the strongly interacting regime, a large drop in the transition temperature is observed. It is worth noting that the thermoresponsive transition point in the strongly interacting regime is closest in value to that

of the PNIPAM homopolymer. At pH 6.4 where strong electrostatic interactions form large complex coacervates, the PNIPAM blocks are predominantly located on the outside of the micelles, promoting PNIPAM-PNIPAM interactions and leading to a cloud point transition similar to that observed in the homopolymer PNIPAM solution at the same pH condition.

In preparing a biofunctional film, preservation of protein activity and control over protein immobilization or release is critical to the end use of the material. Films cast at pH = 6.4 and r_m = 14.2 were chosen for retention and release experiments due to the high loading of mCherry in the PND film without macrophase separation. Optical activity assays of mCherry from the thin films were performed to quantify the functionality of released protein at 40 °C, above the LCST of PNIPAM in the PND and mCherry system. The concentration of mCherry remaining in the film was calculated by the measurement of fluorescence intensity of the solution at 25 °C, where the remaining film was totally dissolved. Two different calibration curves were used for determining the released and remaining mCherry concentrations, because the fluorescence intensity decreases in the presence of PND chains, as illustrated in Figure S4 (see Supporting Information for calibration curves). Figure 7a shows the pH sensitivity of the hybrid films on release of mCherry at 40 °C. At pH 9.2 and 7.8, the release rates are 10 times faster than at pH 6.4, where relatively strong electrostatic interactions exist between the protonated amine groups in the block copolymer and the net negative surface charge of the protein. However, the release rate slows dramatically after several hours for the high pH conditions, suggesting that some fraction of the mCherry may be maintained in the film under these conditions for extended periods of time. The mCherry release profiles can be fit with a power law function over a period of 4 hr.[55]

$$\frac{M_t}{M_\infty} = kt^n$$

where M_t and M_∞ are the amount of mCherry released at time t and infinite time, respectively. The constant parameter k relates to the structure and geometry specific to the mCherry-PND system, and n represents interactions of the release mechanism. The values of n were determined to be 0.42, 0.37, and 0.31 for pH 6.4, 7.8, and 9.2, respectively. Because the calculated n values are all between 0.5 (diffusion-controlled release) and 0.1 (swelling-controlled release), the release of mCherry in the film as a function of pH appears to be governed by a combination of the disruption of the electrostatic interactions between mCherry and PND and diffusion. Disruption of electrostatics (swelling-controlled release) is more predominant at higher pH, while behavior closer to ideal diffusion-controlled release is observed at lower pH.

Quantifying the concentration of active mCherry remaining in the film allows measurement of the fraction of protein activity retained in the films after casting. The concentration of mCherry remaining in the film is shown in Figure 7b; at each pH condition, the concentration is observed to asymptotically decay as a function of time. Figure 7c shows the concentration of inactive mCherry under the different processing conditions, obtained by subtracting the released and remaining mCherry from the known initial mCherry loading. Independent of pH, a large majority of the protein (~80%) remains active even after having

been dehydrated in vacuum and confined in the films. By comparison, lyophilization of mCherry results in a drop to 15% of the original activity. It can be concluded that the coacervate core composed of PDMAEA has a stabilizing effect that preserves the activity of encapsulated proteins due to the water-based and mild pH processing conditions, and that a stabilizing nanoscale environment is preserved within the coacervate even after water is removed.

CONCLUSIONS

A new method for templating protein self-assembly in block copolymer thin films was demonstrated using all-aqueous processing to preserve protein structure. Controlled RAFT polymerization is employed to synthesize PNIPAM-b-PDMAEA diblock copolymers that microphase separate and complex proteins. Ionic interactions between the surface charges of the model protein mCherry and the cationic PDMAEA block of PND block copolymers were used to drive templating, while the thermoresponsive transition of PNIPAM allowed the films to be stabilized in aqueous environments at elevated temperatures. Complex formation was confirmed by shifts in the absorption spectrum of mCherry, and DLS and zeta potential measurements illustrated that large coacervate micelles form at pH < 6, while smaller micelles form at pH > 7.9. Protein-block copolymer hybrid films are fabricated through water-based self-assembly and coating onto planar substrates to produce nanostructured materials with a domain spacing that corresponds to the coacervate micelle sizes in solution. The amount of mCherry released and loss of protein activity were measured in films heated to 40 °C where PNIPAM was phase-separated and stabilized above the LCST of the homopolymer. At pH 9.2 and 7.8, the release rates are at least 10 times faster than one at pH 6.4 due to deprotonation of PDMAEA. Independent of the pH, the majority of the protein (80%) retains its activity even after having been dehydrated in vacuum and confined in the films.

Supplementary Material

Refer to Web version on PubMed Central for supplementary material.

Acknowledgments

This work was supported by the MIT Energy Initiative (award number 015728-066). Ellipsometry, GPC, and Zeta potential experiments were performed at the MIT Institute for Soldier Nanotechnology. NMR experiments were performed at the MIT Department of Chemistry Instrumentation Facility, and DLS experiments were performed at the Biophysical Instrumentation Facility for the Study of Complex Macromolecular Systems (NSF-0070319 and NIH GM68762). The authors thank Michael Strano in Chemical Engineering at MIT for generous use of the SFM and plate reader. We kindly thank John Ngo for sharing the mCherry gene.

REFERENCES

1. Su XF, Kim BS, Kim SR, Hammond PT, Irvine DJ. Acs Nano. 2009; 3(11):3719–3729. [PubMed: 19824655]
2. Presley AD, Chang JJ, Xu T. Soft Matter. 2011; 7(1):172–179.
3. Cresce AV, Silverstein JS, Bentley WE, Kofinas P. Macromolecules. 2006; 39(17):5826–5829.
4. Rapp BE, Gruhl FJ, Lange K. Analytical and Bioanalytical Chemistry. 2010; 398(6):2403–2412. [PubMed: 20563563]

5. Rahman MM, Ahammad AJS, Jin JH, Ahn SJ, Lee JJ. Sensors. 2010; 10(5):4855–4886. [PubMed: 22399911]
6. Ziegler C, Gopel W. Current Opinion in Chemical Biology. 1998; 2(5):585–591. [PubMed: 9818183]
7. Rogers KR. Analytica Chimica Acta. 2006; 568(1 – 2):222–231. [PubMed: 17761264]
8. Yu EH, Scott K. Energies. 2010; 3(1):23–42.
9. Minteer SD, Liaw BY, Cooney MJ. Current Opinion in Biotechnology. 2007; 18(3):228–234. [PubMed: 17399977]
10. Cracknell JA, Vincent KA, Armstrong FA. Chemical Reviews. 2008; 108(7):2439–2461. [PubMed: 18620369]
11. Patel RN. Coordination Chemistry Reviews. 2008; 252(5 – 7):659–701.
12. Favre N, Christ ML, Pierre AC. Journal of Molecular Catalysis B-Enzymatic. 2009; 60(3 – 4):163–170.
13. Strohmeier GA, Pichler H, May O, Gruber-Khadjawi M. Chemical Reviews. 2011; 111(7):4141–4164. [PubMed: 21553913]
14. Cogdell RJ, Gall A, Kohler J. Quarterly Reviews of Biophysics. 2006; 39(3):227–324. [PubMed: 17038210]
15. Das R, Kiley PJ, Segal M, Norville J, Yu AA, Wang LY, Trammell SA, Reddick LE, Kumar R, Stellacci F, Lebedev N, Schnur J, Bruce BD, Zhang SG, Baldo M. Nano Letters. 2004; 4(6):1079–1083.
16. Valsesia A, Colpo P, Manneill I, Mornet S, Bretagnol F, Ceccone G, Rossi F. Analytical Chemistry. 2008; 80(5):1418–1424. [PubMed: 18220369]
17. Maheshwari G, Brown G, Lauffenburger DA, Wells A, Griffith LG. Journal of Cell Science. 2000; 113(10):1677–1686. [PubMed: 10769199]
18. Xia YN, Rogers JA, Paul KE, Whitesides GM. Chemical Reviews. 1999; 99(7):1823–1848. [PubMed: 11849012]
19. Christman KL, Enriquez-Rios VD, Maynard HD. Soft Matter. 2006; 2(11):928–939.
20. Falconnet D, Pasqui D, Park S, Eckert R, Schift H, Gobrecht J, Barbucci R, Textor M. Nano Letters. 2004; 4(10):1909–1914.
21. Laaksonen P, Kivioja J, Paananen A, Kainlauri M, Kontturi K, Ahopelto J, Linder MB. Langmuir. 2009; 25(9):5185–5192. [PubMed: 19253945]
22. Thomas CS, Glassman MJ, Olsen BD. Acs Nano. 2011; 5(7):5697–5707. [PubMed: 21696135]
23. Le Droumaguet B, Mantovani G, Haddleton DM, Velonia K. Journal of Materials Chemistry. 2007; 17(19):1916–1922.
24. Velonia K, Rowan AE, Nolte RJM. Journal of the American Chemical Society. 2002; 124(16): 4224–4225. [PubMed: 11960447]
25. Segalman RA. Materials Science & Engineering R-Reports. 2005; 48(6):191–226.
26. Hawker CJ, Russell TP. Mrs Bulletin. 2005; 30(12):952–966.
27. Bates FS, Fredrickson GH. Physics Today. 1999; 52(2):32–38.
28. Albert JNL, Epps TH. Materials Today. 2010; 13(6):24–33.
29. Erickson HP. Biological Procedures Online. 2009; 11(1):32–51. [PubMed: 19495910]
30. Matsusaki M, Omichi M, Kadowaki K, Kim BH, Kim SO, Maruyama I, Akashi M. Chemical Communications. 2010; 46(11):1911–1913. [PubMed: 20198250]
31. Lau KHA, Bang J, Kim DH, Knoll W. Advanced Functional Materials. 2008; 18(20):3148–3157.
32. Kumar N, Parajuli O, Hahm JI. Journal of Physical Chemistry B. 2007; 111(17):4581–4587.
33. Zhao XJ, Zhang SG. Chemical Society Reviews. 2006; 35(11):1105–1110. [PubMed: 17057839]
34. Jones MN. Chemical Society Reviews. 1992; 21(2):127–136.
35. Lindhoud S, de Vries R, Norde W, Cohen Stuart MA. Biomacromolecules. 2007; 8(7):2219–2227. [PubMed: 17530889]
36. Harada A, Kataoka K. Macromolecules. 1998; 31(2):288–294.
37. Cooper CL, Dubin PL, Kayitmazer AB, Turksen S. Current Opinion in Colloid & Interface Science. 2005; 10(1 – 2):52–78.

38. Smith AE, Xu XW, McCormick CL. Progress in Polymer Science. 2010; 35(1 – 2):45–93.
39. Kostiainen MA, Pietsch C, Hoogenboom R, Nolte RJM, Cornelissen J. Advanced Functional Materials. 2011; 21(11):2012–2019.
40. Schild HG. Progress in Polymer Science. 1992; 17(2):163–249.
41. Feil H, Bae YH, Feijen J, Kim SW. Macromolecules. 1993; 26(10):2496–2500.
42. Moad G, Rizzardo E, Thang SH. Australian Journal of Chemistry. 2005; 58(6):379–410.
43. You Y-Z, Oupicky D. Biomacromolecules. 2007; 8(1):98–105. [PubMed: 17206794]
44. Shaner NC, Campbell RE, Steinbach PA, Giepmans BNG, Palmer AE, Tsien RY. Nature Biotechnology. 2004; 22(12):1567–1572.
45. Lee YJ, Erazo-Oliveras A, Pellois JP. Chembiochem. 2010; 11(3):325–330. [PubMed: 20029930]
46. Rowell PP, Chiou CY. Journal of Medicinal Chemistry. 1976; 19(2):300–303. [PubMed: 1082511]
47. Mattison KW, Dubin PL, Brittain IJ. Journal of Physical Chemistry B. 1998; 102(19):3830–3836.
48. Dobrynin AV. Macromolecules. 2005; 38(22):9304–9314.
49. Pletnev S, Subach FV, Dauter Z, Wlodawer A, Verkhusha VV. Journal of the American Chemical Society. 2010; 132(7):2243–2253. [PubMed: 20121102]
50. Shu X, Shaner NC, Yarbrough CA, Tsien RY, Remington SJ. Biochemistry. 2006; 45(32):9639–9647. [PubMed: 16893165]
51. Kneen M, Farinas J, Li YX, Verkman AS. Biophysical Journal. 1998; 74(3):1591–1599. [PubMed: 9512054]
52. Violot S, Carpentier P, Blanchoin L, Bourgeois D. Journal of the American Chemical Society. 2009; 131(30):10356–10357. [PubMed: 19722611]
53. Pei Y, Chen J, Yang LM, Shi LL, Tao Q, Hui BJ, Li R. Journal of Biomaterials Science-Polymer Edition. 2004; 15(5):585–594. [PubMed: 15264660]
54. Liu RX, Fraylich M, Saunders BR. Colloid and Polymer Science. 2009; 287(6):627–643.
55. Korsmeyer RW, Gurny R, Doelker E, Buri P, Peppas NA. International Journal of Pharmaceutics. 1983; 15(1):25–35.

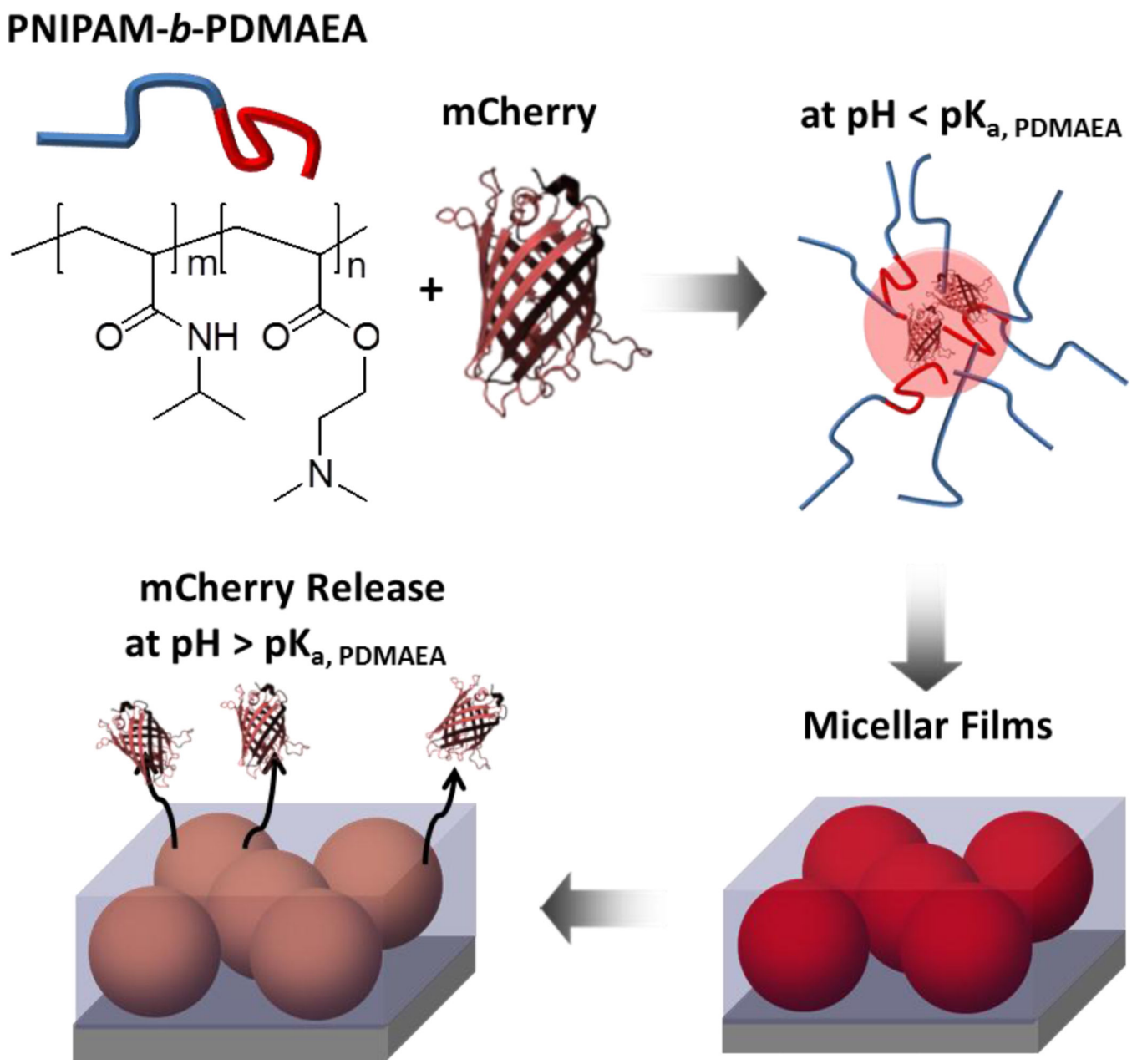

Figure 1.

Formation of coacervate micelles consisting of PNIPAM-*b*-PDMAEA (PND) block copolymers and the red fluorescent protein mCherry enables templating of proteins into polymer thin films under aqueous conditions. Release or immobilization of the proteins from the films may be stimulated by pH and temperature changes.

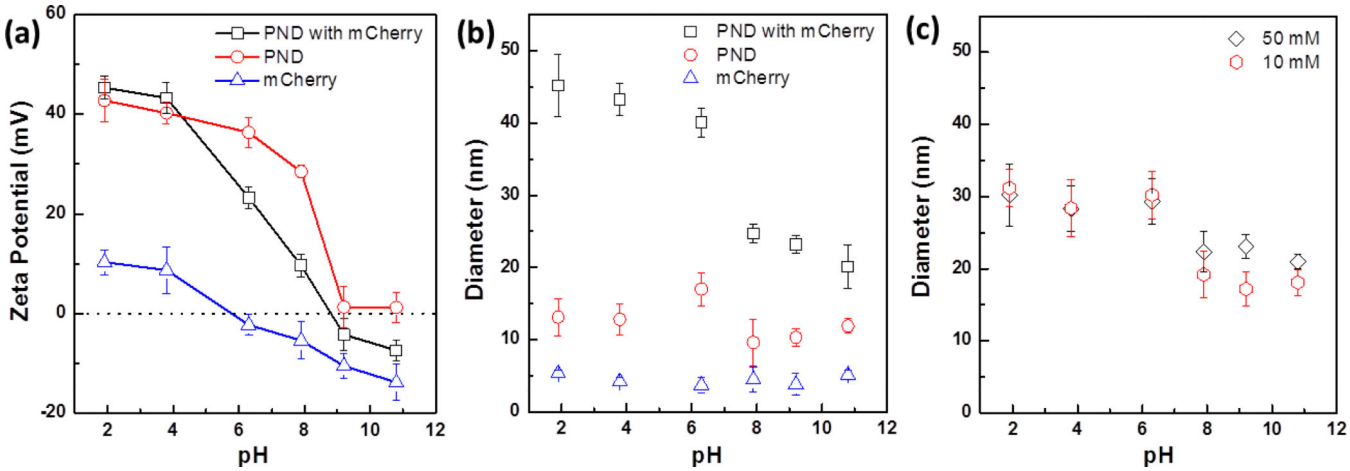

Figure 2.

(a) Zeta potential of aqueous solutions of mCherry, PND, and PND/mCherry complexes as a function of pH. Hydrodynamic diameter observed by dynamic light scattering (DLS) of (b) aqueous solutions of mCherry, PND, and PND/mCherry complexes in the absence of salt and (c) 10 and 50 mM phosphate buffer solutions of PND/mCherry complexes. All experiements were performed in 1 mg/ml solutions at r_m = 14.2 at 25 °C. Particle size increases rapidly between pH 7.9 and pH 6.0 where the PDMAEA and mCherry have strong attractive interactions due to opposite charge.

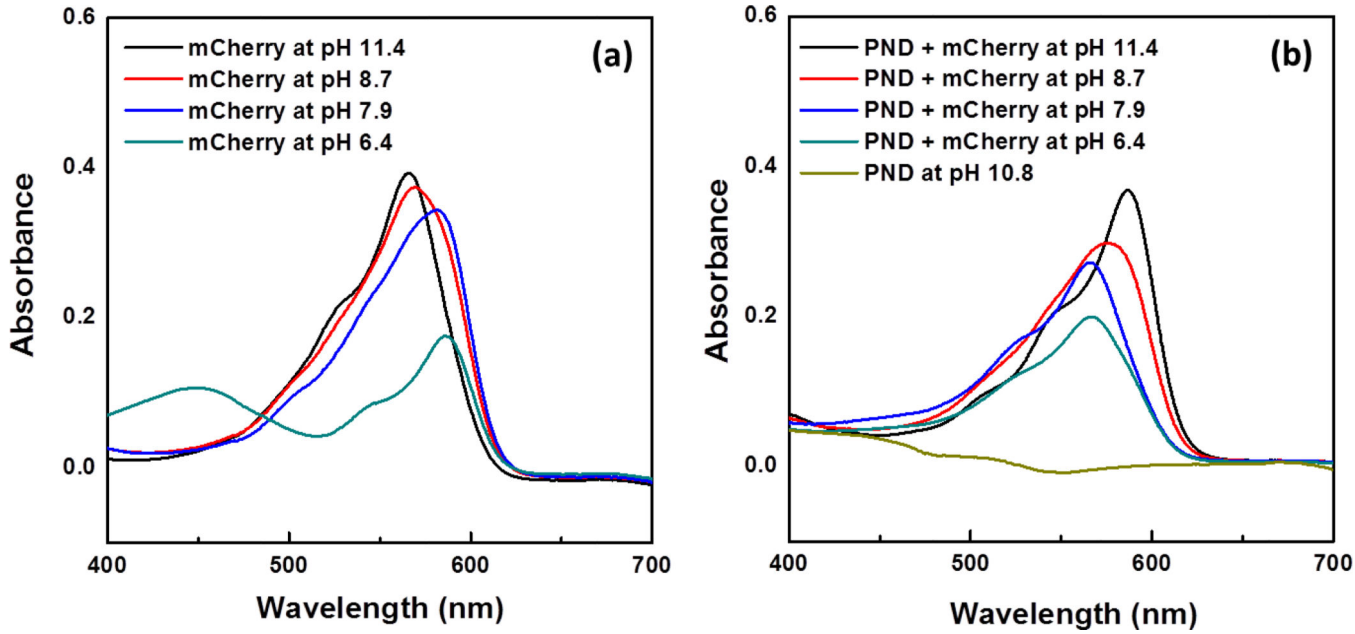

Figure 3.

Solution-state UV-Vis spectra of (a) mCherry (12 nmol/ml) and (b) mCherry (12 nmol/ml) and PND (170 nmol/ml) mixtures with changing pH. The primary absorbance peak of mCherry blue shifts as pH increases, but in the presence of PND, the primary absorbance peak red shifts with increasing pH, owing to electrostatic interactions between the protein and the PDMAEA block. mCherry concentration is equal in all samples.

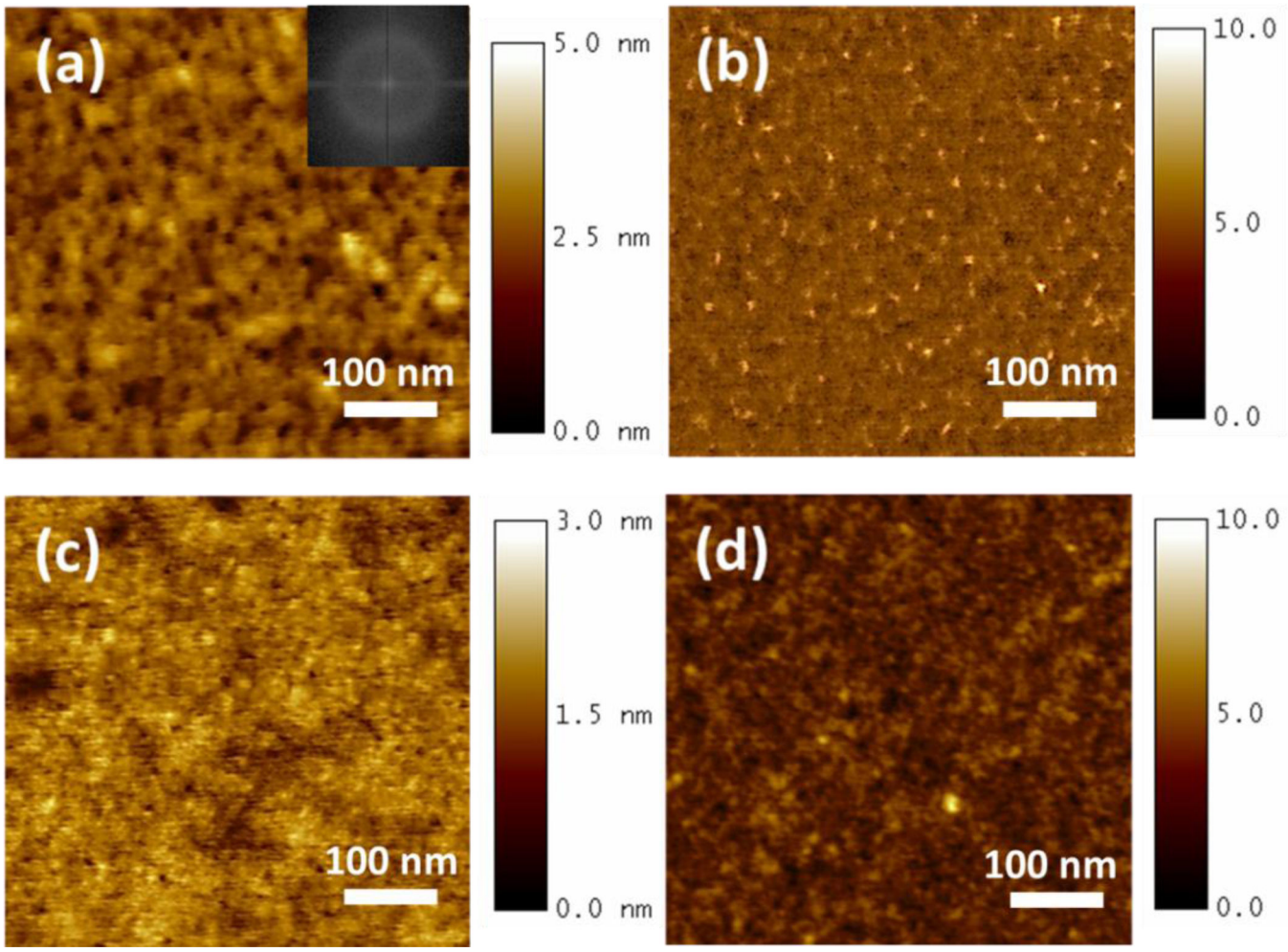

Figure 4.

SFM height images of the PND and mCherry films cast from 2 wt.% solutions at pH (a) 6.4 and (c) 9.2. (b) and (d) are the corresponding phase images. The inset is the fast Fourier transforms of Figure 4 (a).

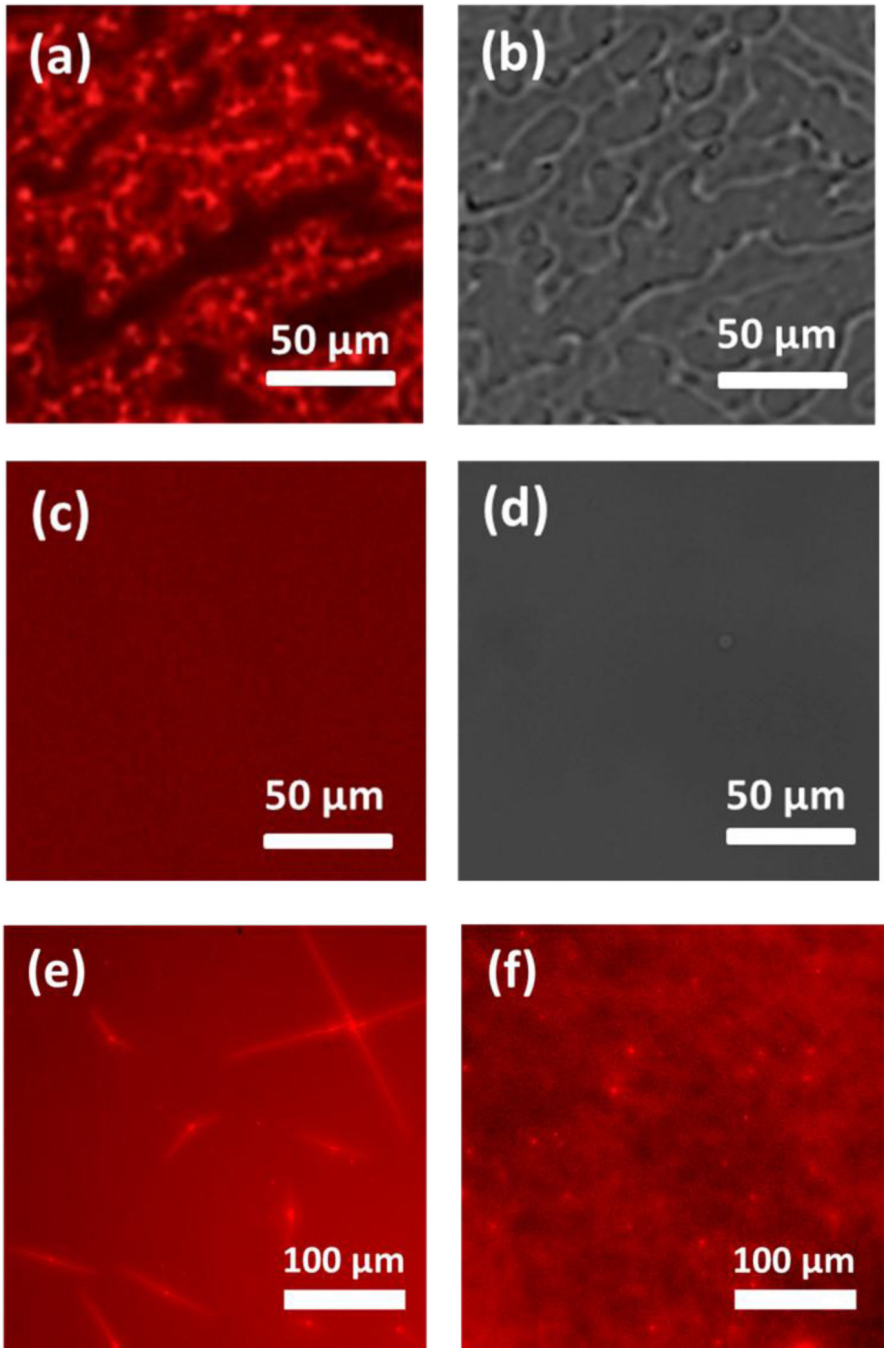

Figure 5.

(a) Fluorescence and (b) bright-field images of PNIPAM and PDMAEA blend film with mCherry. (c) Fluorescence and (d) bright-field images of PND diblock copolymer film with mCherry (molar ratio of polymer to protein, r_m = 14.2). Both the blend and block copolymer films were cast at a pH of 6.4. Macrophase separation is observed between the PNIPAM and PDMAEA homopolymer blend with mCherry segregating into the PDMAEA domain. Microphase separation and complexation with mCherry in the PND-mCherry film produces

a microscale homogeneous structure. Fluorescence images of PND with mCherry (e) at r_m of 2.8, cast from pH 6.4 solution and (f) at r_m of 14.2, cast from pH 9.2.

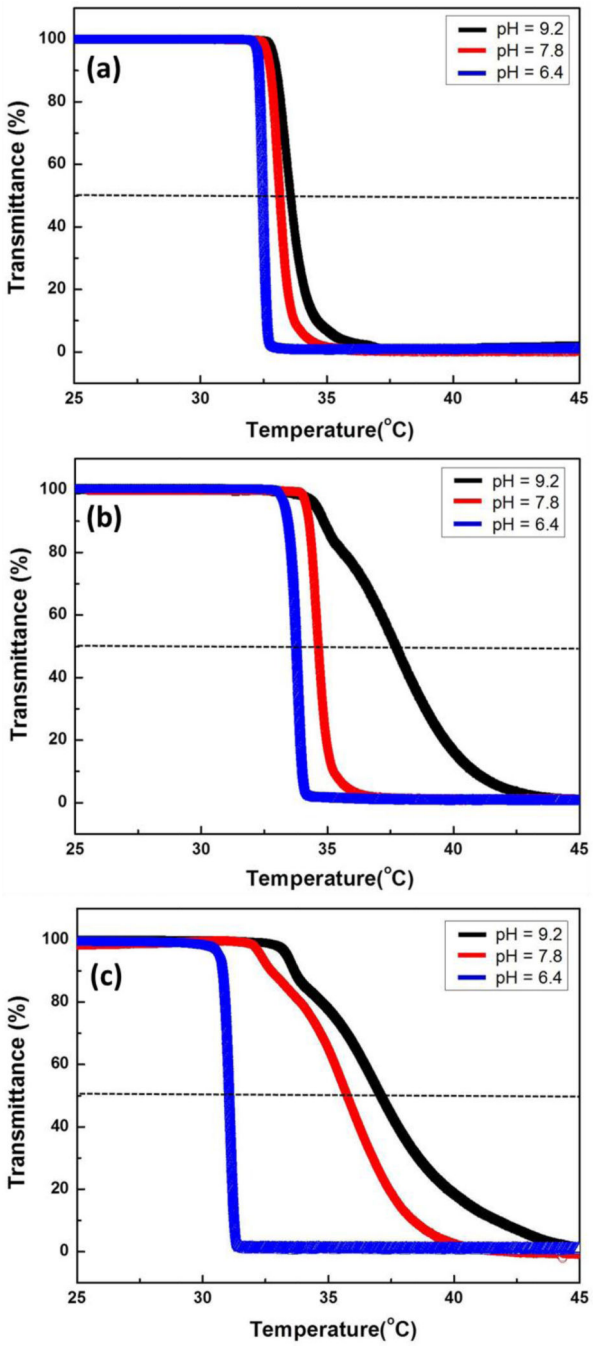

Figure 6.

Effect of pH on the thermosensitive solubility of (a) PNIPAM homopolymers, (b) PND, and (c) PND and mCherry in 10 mM sodium phosphate buffers. Transmission is measured at 450 nm, outside the absorption band of mCherry. The sweep rate is 0.2 °C /min.

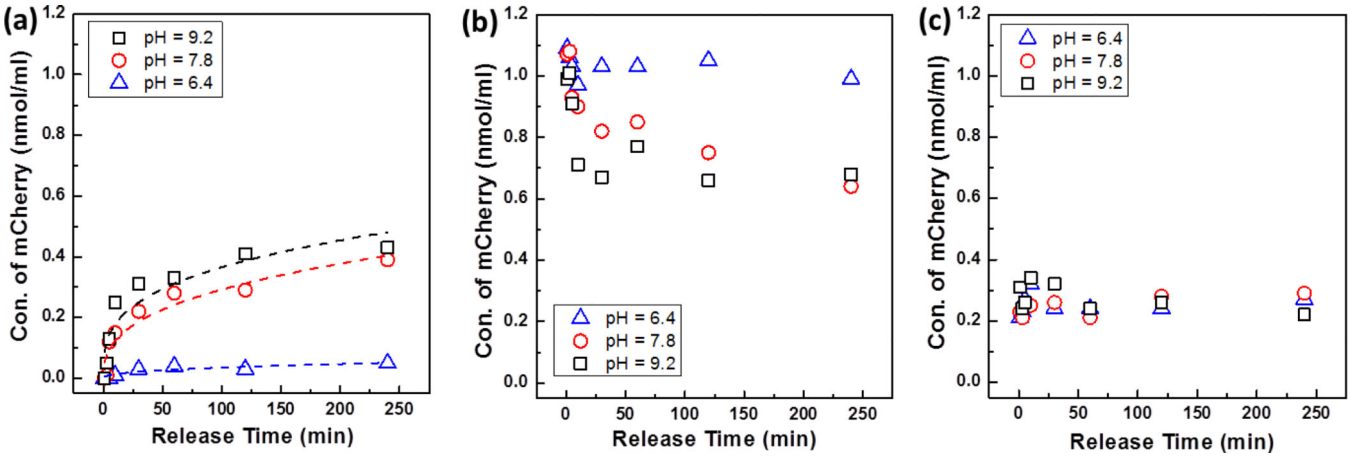

Figure 7.

(a) pH- dependent release of mCherry from the hybrid films at 40 °C. (b) Concentration of active mCherry remaining in the films. (c) Concentration of inactive mCherry under the processing conditions. Independent of pH, the majority of the protein (~80%) remains active. Dashed lines indicate power law fits to the protein release model.